May 2015

Using a Semiprognostic Test to Elucidate Key Model Errors of Warm Rain Processes Within a Unified Parameterization of Clouds and Turbulence

Justin Kyle Weber
University of Wisconsin-Milwaukee

Using a Semiprognostic Test to Elucidate Key Model Errors of Warm Rain Processes Within a Unified Parameterization of Clouds and Turbulence

by

Justin K. Weber

A Thesis Submitted in

Partial Fulfillment of the

Requirements for the Degree of

Master of Science

in

Mathematics

at

The University of Wisconsin–Milwaukee

May 2015

Abstract

Using a Semiprognostic Test to Elucidate Key Model Errors of Warm Rain Processes Within a Unified Parameterization of Clouds and Turbulence

by

Justin K. Weber

The University of Wisconsin–Milwaukee, 2015
Under the Supervision of Professor Vincent E. Larson

The representation of clouds and turbulence remains one of the foremost challenges in modeling earth's climate system and continues to remain one of the greatest sources of uncertainty in future climate projections. Increased attention has been given to unifying cloud and turbulence parameterizations in order to avoid the artificial categorization of cloud and turbulence regimes. One such unified parameterization is known as the Cloud Layers Unified by Binormals (CLUBB). CLUBB is a single column model of clouds and turbulence that assumes subgrid scale variability can be represented by a joint probability density function (PDF) of temperature, moisture, momentum, and hydrometeors. An advantage of CLUBB's joint-PDF is that it allows for the interaction of microphysics and subgrid variability which may be important in unified parameterizations.

In order to improve any parameterization, like CLUBB, 'key' model errors must first be diagnosed. This is complicated by numerous feedbacks within the model. In order to elucidate 'key' errors in CLUBB's representation of warm-rain processes, a semiprognostic test was performed in which CLUBB's joint-PDF was supplied with 'perfect' moments derived from a cloud resolving model. An idealized case of the transition from shallow to deep convection over land was used. It was shown that CLUBB's assumed correlations between hydrometeors play a major role in

CLUBB's microphysical budgets. It was also shown that for highly skewed cases, CLUBB's current joint-PDF closure may inadequately represent the marginals of the subgrid scale atmopheric state. Finally, CLUBB's assumption that the skewness of temperature and moisture are proportional to the skewness of vertical velocity may break down in highly skewed cases such as the one tested here.

JMJ

Table of Contents

List of Figures

List of Tables

Acknowledgements

With sincere gratitude, I thank Vince Larson for his support and mentorship, Brian Griffin and Eric Raut for their many contributions and suggestions, Rachel Storer for her initial work on CLUBB's deep convective capabilities and May Wong for assistance in adding scalar budgets.

Chapter 1

Introduction

1.1 Necessity of Cloud Parameterization

Due to computational restraints, general circulation models (GCMs) are typically run with a horizontal resolution on $O(100\ km)$ and coarse vertical resolution. Therefore, many important processes occur on the unresolved, sub-grid scale (SGS) and must be parameterized. Parameterization attempts to represent the important effects that SGS processes have on the larger, resolved scale. Turbulence, and its visible component, clouds, constitute just some of these important SGS processes.

When one considers the complexity of parameterizing clouds and turbulence, it is no surprise that the rate of improvement of cloud and turbulence parameterizations has benn relatively slow. Randall et al. (2003) highlighted some of the complexity facing the parameterization development community and Randall (2013) summarized some of the recent improvements and the current approaches to tackling the "cloud parameterization problem". In general, the long standing problem of parameterizing clouds and turbulence in GCMs continues to persist. According to the latest report by the Intergovernmental Panel on Climate Change, clouds continue to remain one of the largest sources of uncertainty in the present suite of climate simulations (Boucher et al., 2013).

Jakob (2014) and Jakob (2010) highlight the challenging nature of improving cloud parameterizations. The diagnosis and alleviation of 'key' errors that lead to substantial improvements often take much longer than the simple identification of a symptom. Futhermore, Jakob (2014) argues that, although the scope of climate

models continues to increase by adding more physical processes, the parameterization development community should not lose focus on improving the parameterization of clouds and turbulence as they are a long standing and critically important problem.

1.2 CLUBB Background

Traditionally, different parameterizations are used for different SGS phenomenon. Oftentimes these phenomenon are artificially categorized. For example, there may be one parameterization for deep convective clouds and another for shallow cumulus clouds. It is easy to imagine where the framework of *different schemes for different regimes* is undesirable; such as the transition from shallow to deep moist convection (DMC) where it may not be clear where one regime ends and another begins. Increased attention has been given to unifying the parameterization of clouds, that is, a parameterization that treats all cloud types. The need for which is plainly visible and theoretically appealing (Arakawa, 2004). One such unified parameterization is known as the Cloud Layers Unified by Binormals (CLUBB) .

CLUBB is a single-column model of clouds and turbulence. The prognostic equations are based on the Navier-Stokes advection/diffusion equations. It uses an assumed joint probability density function (PDF) to represent SGS variability. It assumes a mixture of two Gaussian distributions for liquid water potential temperature, θ_l, total water (vapor + cloud) mixing ratio, r_t, and vertical velocity, w (Golaz et al., 2002; Larson et al., 2005). CLUBB's PDF has been extended to include mixing ratios and number concentrations of rain, snow, graupel, and cloud-ice, which are represented as a mixture of two Delta-Lognormal distributions (where the precipitation free region is represented as a Delta function) (Larson and Griffin, 2013; Griffin and Larson, 2013). CLUBB's joint PDF can be written as $P(\theta_l, r_t, w, N_c, r_r, N_r, r_s, N_s, r_g, N_g, r_i, N_i,) = aP(...)_1 + (1-a)P(...)_2$. Where $P(...)_1$

and $P(...)_2$ refer to the first and second 'components' of the PDF, a is a mixture fraction and N_x and r_x represent the number concentrations and mixing ratios, respectively, for some hydrometeor species where the subscripts c, r, s, g, i, refer to cloud, rain, snow, graupel, and cloud-ice, respectively.

A chief advantage of CLUBB's joint-PDF is that it allows for the interaction of the variability of the SGS state (θ_l, r_t, and w) with microphysics. This is critically important since microphysical processes are largely nonlinear and that by using grid cell mean quantities, rather than taking SGS variability into account, one would arrive at biased estimates in grid cell mean microphysical tendencies (Larson et al., 2001b). That is, for a nonlinear function $f(x)$, $\overline{f(x)} \neq f(\overline{x})$. In order to drive microphysics with SGS variability, CLUBB's joint-PDF is sampled using a Monte-Carlo type approach called the Subgrid Importance Latin Hypercube Sampler (SILHS) (Larson et al., 2005; Larson and Schanen, 2013). SILHS constructs a sample column consistent with CLUBB's joint-PDF. This sample column could be conceptualized as a subcolumn of a GCM's grid cell. Each subcolumn is then fed into a microphysics scheme one by one. The resulting tendencies are then averaged appropriately. Latin hypercube sampling ensures the joint-PDF is sampled evenly. That is, sample points are not clustered. CLUBB also has the option of sampling preferentially in-cloud ("Subgrid Importance") and appropriately weighting the samples. This can help reduce the computational cost since feeding multiple sub-columns through the microphysics scheme is computationally expensive.

Bogenschutz et al. (2013) replaced the default boundary layer, shallow convection, and cloud macrophysics parameterizations with CLUBB in the Community Atmosphere Model, version 5. They showed an improvement in the transition from stratocumulus to cumulus in the subtropics. They attributed this improvement to CLUBB's unified nature which allows turbulence to evolve rather than be treated by different parameterization schemes which can lead to abrupt transitions. In

a single column framework, Storer et al. (2015) included the effects of ice latent heating and improved the turbulent transport of hydrometeors in CLUBB, features thought necessary to faithfully parameterize DMC. There, they showed CLUBB was capable of simulating deep convective, shallow trade wind cumulus, and drizzling stratocumulus clouds reasonably with a unified scheme.

The advantages and disadvantages of CLUBB has been reported by Golaz et al. (2002) and Larson et al. (2012). A brief summary of theirs follows. Although the size of the code is quite large, on the order of 10,000 lines of FORTRAN code, most of the lines are comments, statistics, error-checks, etc. Nevertheless, the size of CLUBB's software may be similiar to the collective size of the parameterizations (shallow cumulus, boundary layer turbulence, etc.) that CLUBB could replace in a GCM. In addition, the large software size is a result of the detailed and well documented nature of the code, making it easier to navigate. CLUBB must predict nine higher order moments and hence, it is relatively computationally expensive. In addition, when using SILHS, the microphysics scheme is called multiple times. The computational expense of CLUBB is mitigated, in part, by the fact it can replace multiple parameterizations. In addition, computational expense can be mitigated by using a longer timestep, or reducing the number of sample points if using SILHS.

1.3 Warm Rain Processes' and Effect on the Transition from Shallow to Deep Moist Convection

The transition from shallow to DMC is a particular challenge in climate modeling (Betts and Jakob, 2002). Observational studies, such as Zhang and Klein (2010), and modeling studies such as and Khairoutdinov and Randall (2006) and Khairoutdinov et al. (2009) suggest that cold pools generated by evaporative cooling of rain and the subsequent boundary layer inhomogeneity may significantly contribute to this

transition and organization of deep convection. This suggests a tight coupling of microphysics, i.e. rain production and evaporation, and SGS variability.

Owing to its unified nature and ability to drive microphysics with SGS variability, CLUBB is well poised to simulate this transition. In Storer et al. (2015), CLUBB struggled with the transition from shallow to DMC, as many parameterizations do, and exhibited a rapid onset of intense precipitation for a brief period of time rather than a gradual increase in the precipitation rate Storer et al. (2015). As mentioned in Bogenschutz et al. (2013), one difficultly in improving unified parameterizations is that it is hard to 'tune-away', in the traditional sense, different biases. A *real* improvement, therefore, is usually the result of a structural change in CLUBB's PDF or improving how CLUBB closes unclosed moments. Before, those changes can be made, however, 'key' model errors must be elucidated.

The focus of this thesis was to improve CLUBB's handling of warm rain processes leading upto and during the transition from shallow to DMC. In Chapter 2, the methodology to diagnose 'key' model errors will be discussed and model configurations of CLUBB and a cloud resolving model (CRM) will be presented. Chapter 3 will first motivate the importance of warm rain processes during the transition from shallow to DMC by examining their effects on higher order moments of θ_l and r_t. Next, possible improvements in CLUBB's representation of warm rain processes will be discussed. Chapter 4 closes with a brief discussion and conclusion.

Chapter 2

Methods

2.1 Semiprognostic Test

Atmospheric models are inherently nonlinear which makes the diagnosis of so called 'key' errors difficult. Oftentimes, an error may cascade throughout the model making the source of the error difficult to identify. In a semiprognostic test (Randall et al., 1997), both the state and tendencies within the atmospheric column are prescribed except for those associated with the processes to be studied and improved. In this way, the model being tested can continually accumulate errors. The largest errors may indicate parts of the model needing acute attention.

CLUBB's statistical nature allows for an easy implementation of a semiprognostic test. However, many of CLUBB's moments are difficult or nearly impossible to observed directly in nature. To provide 'perfect' moments, we use a CRM as 'truth'. The CRM used is the System for Atmospheric Modeling (SAM, Khairoutdinov and Randall (2003)) which has been used to simulate a wide variety of idealized cases. It uses the analestic equations of motion and prognoses liquid water/ice moist static energy, non-precipitating water (vapor + cloud water + cloud ice) and precipitating water (rain + snow + graupel). A grid cell is assumed to be either totally saturated or sub-saturated. SAM was used as a measure of truth since, embedded in a GCM, CLUBB should predict the SGS processes that would be otherwise explicitly resolved if a GCM had a higher spatial resolution. This is a key point. CLUBB should emulate the statistical profiles that would otherwise be explicitly resolved if a GCM were run with sufficient spatial resolution. In this way, CLUBB acts as a

CRM emulator.

The semiprognostic test was performed in the following way. First, profiles of CLUBB's prognosed moments were calculated within SAM and output every minute, which corresponds to CLUBB's timestep. Next, CLUBB was integrated using the same boundary and initial conditions as the SAM simulation. Then, CLUBB's prognosed moments from the SAM simulation are prescribed at the beginning of each CLUBB timestep. That is, $\overline{\theta_l}$, $\overline{r_t}$, $\overline{w}$, $\overline{\theta_l'^2}$, $\overline{r_t'^2}$, $\overline{w'^2}$,$\overline{w'\theta_l'}$, $\overline{w'r_t'}$, $\overline{\theta_l'r_t'}$, and w'^3 is prescribed. Since warm rain processes are of interest, $\overline{r_r}$, $\overline{r_r'^2}$, $\overline{N_r}$, $\overline{N_r'^2}$, $\overline{r_i}$, $\overline{r_i'^2}$, $\overline{N_i}$, $\overline{N_i'^2}$,$\overline{r_s}$,$\overline{r_s'^2}$, $\overline{N_s}$, $\overline{N_s'^2}$, $\overline{r_g}$, $\overline{r_g'^2}$,$\overline{N_g}$,$\overline{N_g'^2}$ were also prescribed and the same microphysics parameterization used in SAM was used in CLUBB. By feeding in 'perfect' moments at the beginning of each CLUBB timestep, the diagnosis of key errors arising from CLUBB's PDF or PDF closure is easier since many of the feedbacks were removed.

2.2 Idealized Case of the Transition from Shallow to DMC

An idealized case of the transition from shallow to DMC was used for the test. Specifically, the case simulated here was taken from the 23-February 1999 case during the Large-Scale Biosphere-Atmosphere - Tropical Rainfall Measuring Mission (LBA-TRMM, referred to as LBA hereafter) ground validation program (Silva Dias et al., 2002). This case has been used in an intercomparison study (Grabowski et al., 2006) and other modeling studies of the transition from shallow to DMC (e.g. Khairoutdinov and Randall (2006)). The simulation starts at 0730 LST. Surface sensible and latent heat fluxes increase throughout the simulated morning to a maximum of 269.9 and 553.8 W m^2, respectively. Radiative heating tendencies are prescribed, although they do not play a significant role owing to the short simulation time.

2.3 Cloud Resolving Model Configuration

SAM's model domain spanned 128 km x 128 km and extended up to 27.8 km. The horizontal grid spacing was 1 km and the vertical grid spacing was stretched, increasing from 25 m to 250 m at 5.8 km and constant thereafter. A timestep of 6 s was used. The simulation is relatively short, only 6 hours long, and starts at 0730 LST. The Morrison et al. (2009) microphysics parameterization, which is a double moment scheme for cloud, rain, snow, graupel (or hail) and cloud-ice, was used. For simplicity, cloud droplet number concentration, N_c, is prescribed to be a constant 100 cm^{-3}. Details of SAM's model configuration can be found in Table 2.1.

Table 2.1: SAM model configuration

	SAM Configuration
Number of vertical grid levels	128
Vertical grid spacing	25-250 m
Horizontal grid spacing	1000 m
Horizontal domain size	128 km
Time step	6 s
Duration	6 hr
Microphysics	Morrison et al. (2009)
N_c	100 cm^{-3}
Radiation	Prescribed

2.4 CLUBB Model Configuration

When possible, CLUBB is configured identically to SAM for the LBA simulation. It uses the same Morrison et al. (2009), initial, and boundary conditions. CLUBB assumes the mean and the variance of the Lognormal distribution is proportional and constant in time and space, that is, $\sigma_i^2 = V_i \mu_i^2$ where σ_i^2 and μ_i^2 are the mean squared and variance of the i^{th} hydrometeor and V_i is their proportionality. Table 2.2 lists V_i used here.

Table 2.2: The prescribed ratio (V_i) between the within-precipitation variance and the mean squared of each hydrometeor.

Variable	Variance Ratio (V_i)
r_r	5.0
N_r	2.5
r_g	1.25
N_g	0.625
r_s	1.25
N_s	0.625
r_i	1.25
N_i	0.625

CLUBB assumes the correlations between temperature, moisture, vertical velocity, and hydrometeors to be constant with time and space. CLUBB uses a transformation of θ_l and r_t called extended liquid water potential temperature, χ and orthogonal extended liquid water potential temperature, η. χ is expressed as (Lewellen and Yoh, 1993),

$$\chi = r_t - r_s \frac{1 + \xi r_t}{1 + \xi r_s}, \tag{2.1}$$

where r_s is the saturation mixing ratio and ξ is expressed as,

$$\xi = \frac{R_d}{R_v} \left(\frac{L_v}{R_d T_l} \right) \left(\frac{L_v}{c_p T_l} \right), \tag{2.2}$$

where R_d and R_v are the gas constants of dry air and water vapor, respectively, c_p is the specific heat of the mixture at constant pressure, L_v is the latent heat of vaporization, and $T_l \equiv \theta_l \left(\frac{p}{p_o} \right)^{R_d/c_p}$ where p_o is some reference pressure (p). χ has the attractive property of being equal to r_c when saturated and is less than zero when sub-saturated. The prescribed correlations can be seen in Table 2.3.

The above variances and correlations are similar to those found in Storer et al. (2015) and were the current default settings for CLUBB. Collectively, this configuration will be referred to as the 'Default' configuration. In order to reduce the

Table 2.3: Correlations used for χ, η, w, N_{cn}, r_r, N_r, r_i, N_i, r_s, N_s, r_g, N_g. Shown are the within-cloud values. For below cloud, another correlation table is use and for our purposes is identical except corr(χ,η) = .3. The correlation matrix is symmetric, so the values below the diagonal are not filled in.

	χ	η	w	N_{cn}	r_r	N_r	r_i	N_i	r_s	N_s	r_g	N_g
χ	1.0	-0.6	0.09	0.09	0.5	0.5	0.2	0.2	0.2	0.2	0.2	0.2
η		1.0	0.027	0.027	0.0726	0.0855	-0.024	0.084	0.018	0.012	0.0	0.0
w			1.0	0.34	0.2	0.2	0.1	0.15	0.0	0.0	0.0	0.0
N_{cn}				1.0	0.0	0.0	0.39	0.29	0.14	0.21	0.0	0.0
r_r					1.0	0.7	0.0	0.0	0.1	0.1	0.2	0.2
N_r						1.0	0.1	0.1	0.0	0.0	0.2	0.2
r_i							1.0	0.7	0.5	0.5	0.3	0.3
N_i								1.0	0.5	0.5	0.3	0.3
r_s									1.0	0.7	0.4	0.4
N_s										1.0	0.4	0.4
r_g											1.0	0.7
N_g												1.0

sensitivity to sampling noise, CLUBB was integrated using 512 subcolumns generated by SILHS.

Chapter 3

Results

3.1 SAM Simulation Overview

An overview of the SAM simulated cloud field can be seen in Figure 3.1. As the simulated morning progresses, the boundary layer deepens and shallow clouds begin to form. These clouds continue to grow in vertical extent throughout the simulated day. Shortly after 200 min, domain mean precipitation rate starts to increase. The first hour of precipitation is driven by warm rain processes, indicated by the blue shading of the lower plot of Figure 3.1. This phase will be referred to as the 'warm phase'. Precipitation rate continues to increase when, by 4.5 hours, a secondary local maximum of $\overline{r_c}$ appears above the freezing level illustrating the transition to deep convection. This latter phase will be referred to as the 'deep phase'.

3.1.1 Sensitivity to Horizontal Resolution

Bryan et al. (2003) studied the resolution requirements for the simulation of DMC. There, they argued that spatial resolution on $O(100$ m) is needed to adequately resolve the turbulent motions in DMC. Perhaps one of their most interesting findings was the lack of convergence of scalar and momentum fluxes with increasing resolution, especially for the weakly sheared environments they simulated. Due to the short duration of the LBA case, it allowed for some exploration of the sensitivity to horizontal resolution. The model configuration is identical to Table 2.1 except for the horizontal resolution and attendant time step. Three additional simulations were performed with horizontal grid spacings of 2 km, 500 m, and 250 m, with

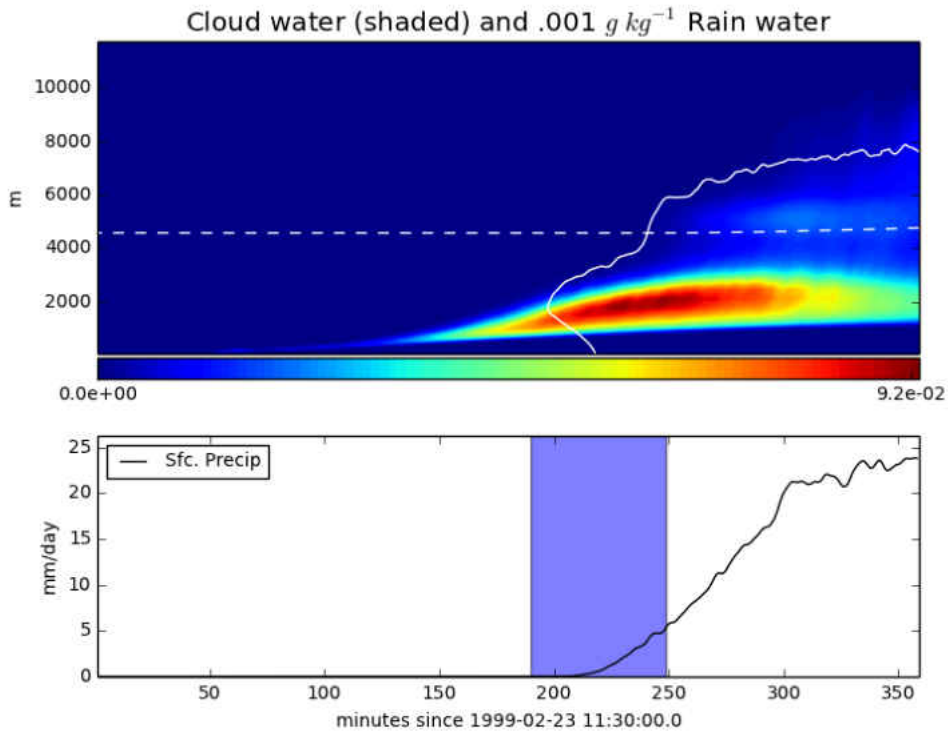

Figure 3.1: Top; domain mean cloud water mixing ratio (shaded), .001 g kg^{-1} rain water mixing ratio (solid white), and height of the 0 ^oC isotherm (dashed white) for the 1 km SAM simulation. Bottom; domain mean precipitation rate. The blue area indicates times where the domain mean precipitation rate was non-zero and domain mean frozen hydrometeor species (graupel or snow) was less than .001 $g\ kg^{-1}$ throughout the column.

timesteps of 6 s, 6 s, and 3 s, respectively.

Figure 3.2 shows the timeseries of liquid water path and rain water path (RWP) for the duration of each simulation. As horizontal resolution increases, the onset of rain formation is delayed. The 250 m simulation's RWP is visually nonzero approximately an hour after the 2 km simulation's RWP becomes nonzero. The delay is 'compensated' by larger RWP later in the simulation such that the time integrated RWP appears similar across all cases. That is, the coarser resolution simulations rain earlier and with less intensity while the high resolution simulations rain later with higher intensity.

Figure 3.3 shows vertical profiles of $\overline{w'\theta_l'}$ and $\overline{w'r_t'}$ for each simulation averaged

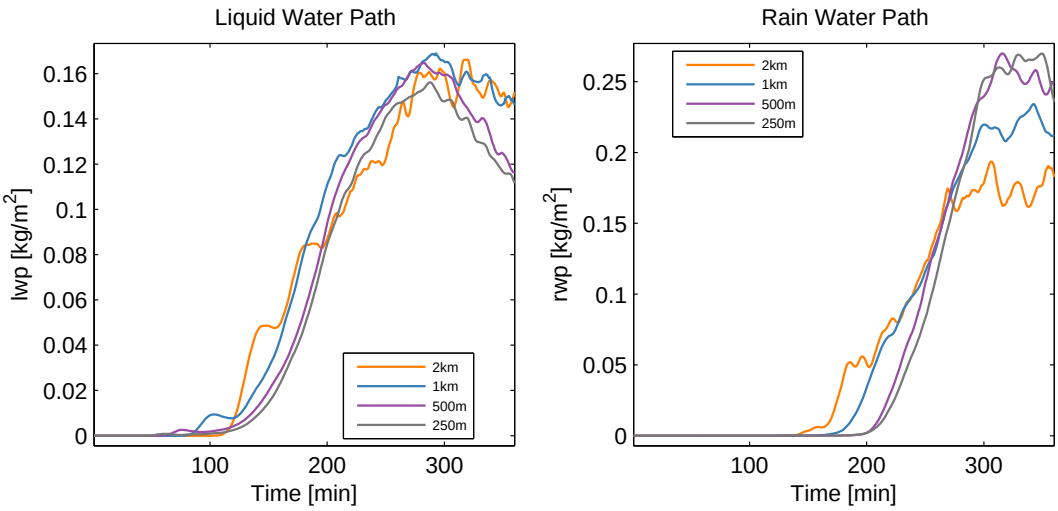

Figure 3.2: Timeseries of LWP (left) and RWP (right) for SAM simulations of varying horizontal resolution.

over both the warm and deep phase (189 - 360 min.) . For both profiles, there does not appear to be a consistent convergence to a 'true' solution with decreasing horizontal resolution.

Figure 3.4 shows the vertical profiles of $\overline{\theta_l'^2}$ and $\overline{r_t'^2}$ averaged over 189 - 360 mins. The variance of r_t systematically decreases with increased horizontal resolution. The same is true for the variance of θ_l except for the peak of $\overline{\theta_l'^2}$ near 2000 m. This peak is associated with the altitude of maximal $\overline{r_c}$, which increases with height with increasing horizontal resolution. However, the statistical profiles are not all that different either.

Inevitably, the question arises as to whether SAM can used as a basis of truth if there doesn't appear to be convergence with increasing horizontal resolution. First of all, the overall details are hardly different between simulations. Each simulation exhibits a deepening boundary layer and shallow clouds preceding a transition to DMC (not shown). In addition, as was argued in Section 2.1, CLUBB should be able to emulate the statistical profiles of SAM (or any CRM). Therefore, in the context of a semiprognostic test, if the moments of CLUBB's joint-PDF corresponds to that of SAM's 1 km simulation, then CLUBB should produce the statistical profiles of

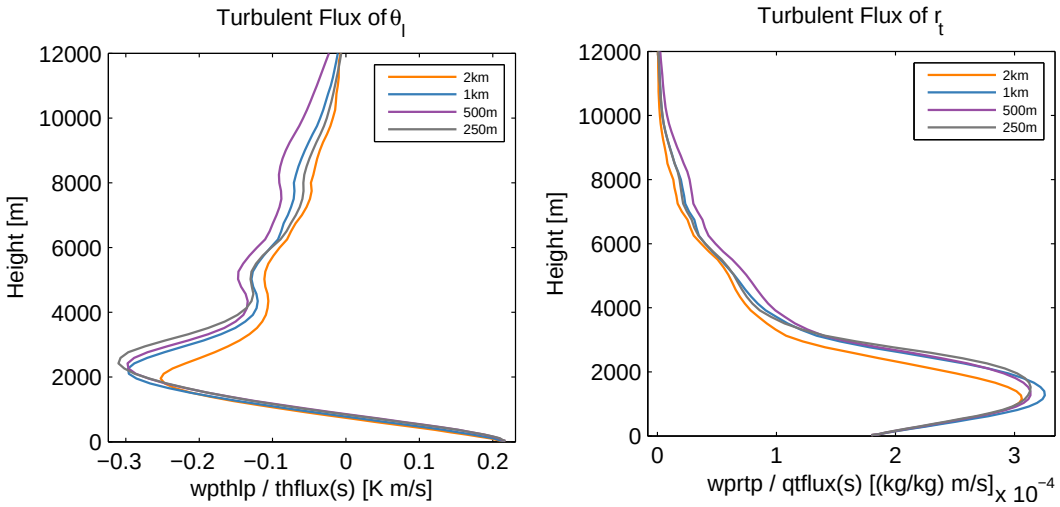

Figure 3.3: As in Figure 3.2 but for vertical profiles of $\overline{w'\theta_l'}$ (left) and $\overline{w'r_t'}$ (right).

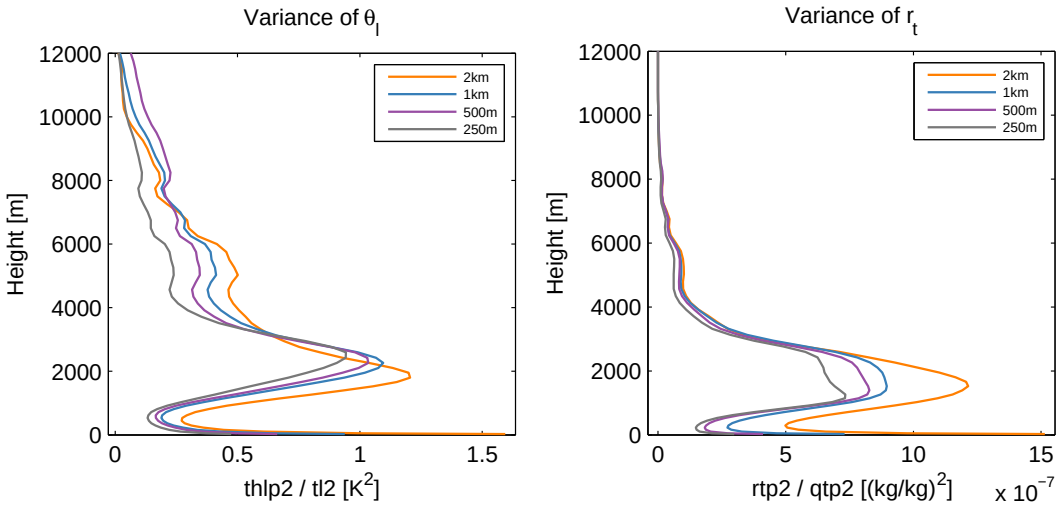

Figure 3.4: As if Figure 3.3, but for $\overline{\theta_l'^2}$ (left) and $\overline{r_t'^2}$ (right)

SAM's 1 km simulation. Since 3D output for the sub-1 km SAM simulations was quite large, and the statistical profiles were similar for each of the simulations, the 1 km simulation was used for the semiprognostic test.

3.2 Higher Order Moments and the Effects of Precipitation

3.2.1 Time-Averaged Mean Profiles

Figure 3.5 shows the time-averaged mean profiles of the domain mean, variance, and turbulent fluxes of $\overline{\theta_l}$ and $\overline{r_t}$ during the warm and deep phase of the simulation. The domain mean profiles do not change very much, which would be expected for such a short simulation. The height of the boundary layer increases from the warm phase to the deep phase. Also, there is a warming and drying of the boundary layer. This is consistent with the typical evolution of the convective boundary layer.

$\overline{\theta_l'^2}$ and $\overline{r_t'^2}$ are relatively large near the surface owing to the prescribed latent and sensible heat fluxes. Immediately above the surface layer, $\overline{\theta_l'^2}$ and $\overline{r_t'^2}$ rapidly decrease owing to efficient turbulent mixing in the boundary layer. $\overline{\theta_l'^2}$ increases from cloud base near the altitude of maximum $\overline{r_c}$ (not shown) and decreases above. A similar profile follows for $\overline{r_t'^2}$, which is maximized within the liquid cloud layer.

Within the boundary layer, $\overline{w'\theta_l'}$ is positive. This illustrates turbulence acting to redistribute the prescribed surface sensible heat flux throughout the boundary layer. At cloud base, $\overline{w'\theta_l'}$ is negative and becomes more negative throughout the depth of the cloudy layer. That is, updrafts are associated with lower values of θ_l (cloudy air). $\overline{w'r_t'}$ is positive throughout.

3.2.2 Budgets of $\overline{\theta_l'^2}$ and $\overline{r_t'^2}$

Although the profiles of $\overline{\theta_l}$ and $\overline{r_t}$ varied little over the course of the short simulation, the higher order moments involving them did change. The processes acting on those higher order moments can were elucidated through a budget analysis. Of particular interest was the magnitude of the precipitation term, especially during the warm phase where clouds were shallow and precipitation was not intense. Budget terms

were calculated within SAM at every timestep and averaged every minute.

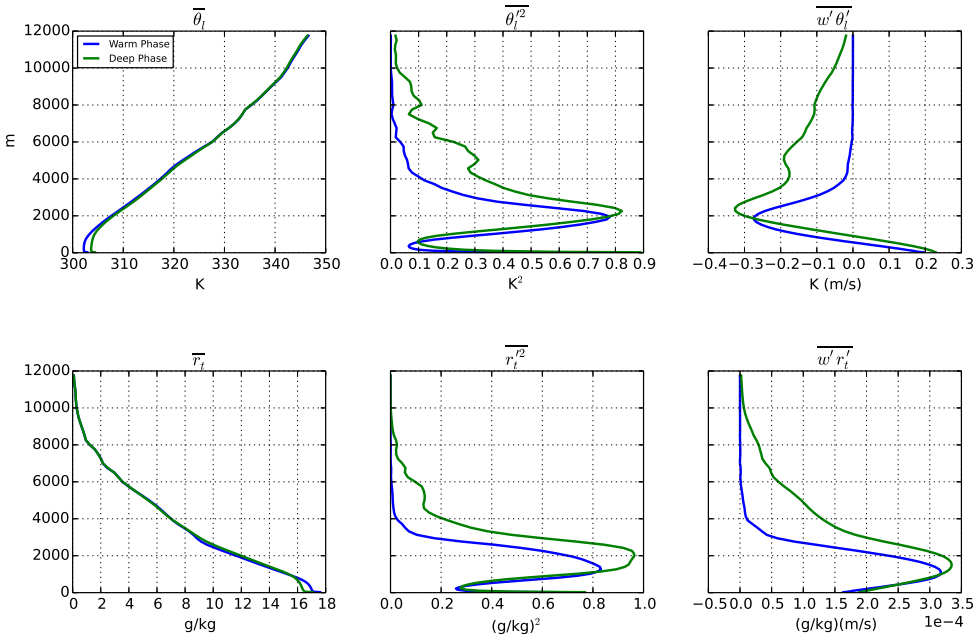

Figure 3.5: Mean vertical profiles of the (from left to right) mean, variance, and flux of $\overline{\theta_l}$ (top) and $\overline{r_t}$ (bottom). The 'Warm Phase' is averaged over minutes 189 - 249 (blue highlight in Figure 3.1) and the 'Deep Phase' is averaged over minutes 249 - 360.

The equation governing the variance of θ_l is written as

$$\frac{\partial}{\partial t}\overline{\theta_l'^2} = \underbrace{-\overline{\rho}^{-1}\frac{\partial}{\partial z}(\overline{\rho}\overline{w'\theta_l'^2})}_{Turbulent Advection} \quad \underbrace{-2\overline{w'\theta_l'}\frac{\partial\overline{\theta_l}}{\partial z}}_{Gradient Production} \quad \underbrace{+\frac{\partial\overline{\theta_l'^2}}{\partial t}|_{prec}}_{Precipitation} \quad \underbrace{-D}_{Dissipation}, \tag{3.1}$$

where ρ is the density of air, $prec$ represents the effects of precipitation on $\theta_l'^2$, and D is dissipation.

The equation governing the variance of r_t is written as (e.g. Khairoutdinov and Randall (2002))

$$\frac{\partial}{\partial t}\overline{r_t'^2} = \underbrace{-\overline{\rho}^{-1}\frac{\partial}{\partial z}(\overline{\rho}\overline{w'r_t'^2})}_{Turbulent Advection} \quad \underbrace{-2\overline{w'r_t'}\frac{\partial\overline{r_t}}{\partial z}}_{Gradient Production} \quad \underbrace{+2\overline{r_t'\left(\frac{\partial r_t}{\partial t}\right)_{prec}}}_{Precipitation} \quad \underbrace{-D}_{Dissipation}. \tag{3.2}$$

Figure 3.6 shows the budgets of $\overline{\theta_l'^2}$ during the warm and deep phase of the simulation. Precipitation always acted to reduce $\overline{\theta_l'^2}$ and is maximized where turbulent advection is positive. In the both phases, the sum of turbulent advection and precipitation largely offset the gradient production leading to a small time tendency of $\overline{\theta_l'^2}$.

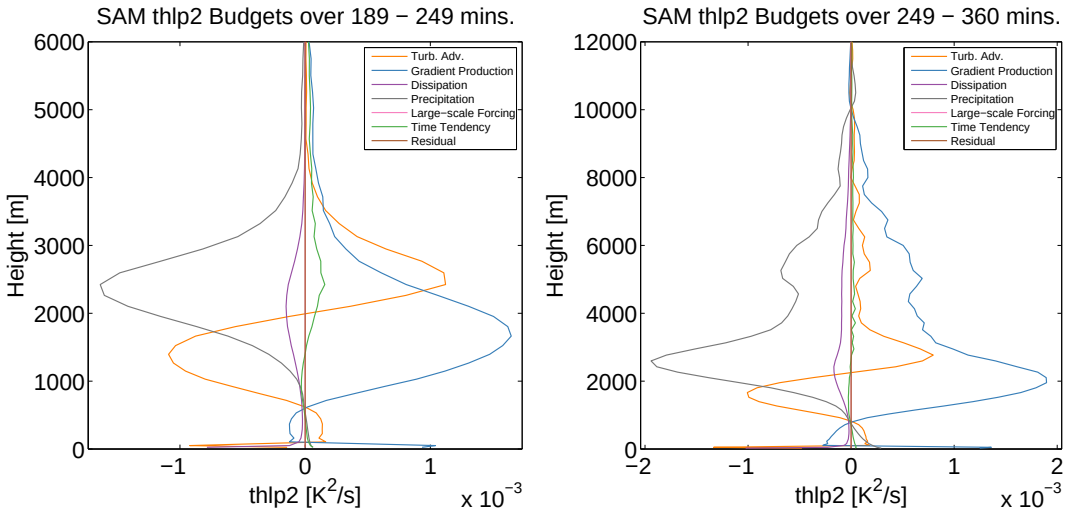

Figure 3.6: Mean vertical profiles of $\overline{\theta_l'^2}$ during the warm phase (left) and deep phase (right). Note the change in scale of altitude.

Figure 3.7 shows the budgets of $\overline{r_t'^2}$ during the warm and deep phase of the simulation. Similar to the budget of $\overline{\theta_l'^2}$, precipitation always acted to reduce the variance and is maximized where the turbulent advection is positive. The sum of turbulent advection and precipitation largely offset the gradient production leading to a small time tendency of $\overline{r_t'^2}$.

3.2.3 Budgets of $\overline{w'\theta_l'}$ and $\overline{w'r_t'}$

A similar budget analysis was performed for the turbulent fluxes of θ_l and r_t. The equation governing the turbulent flux of θ_l is written as

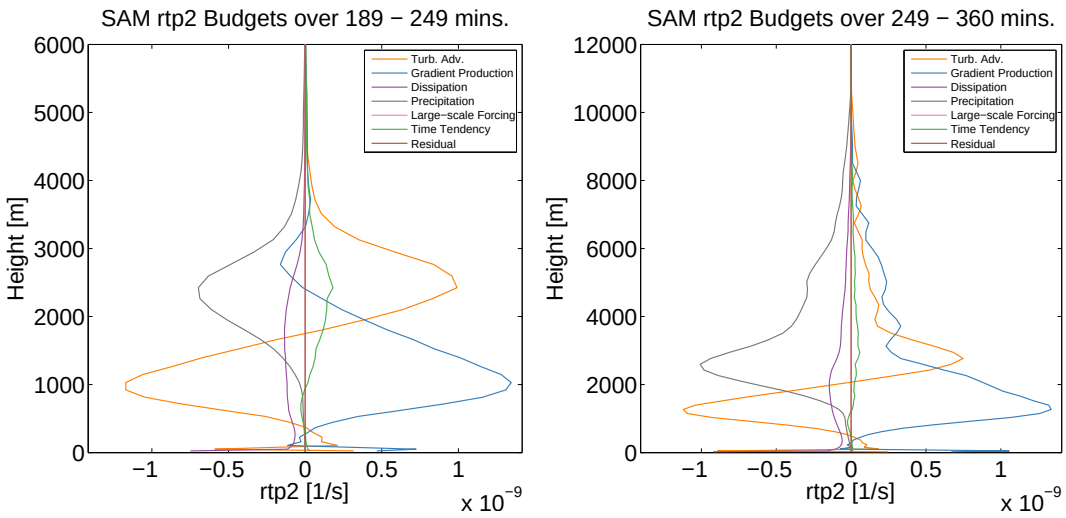

Figure 3.7: As in Figure 3.6 but for $\overline{r_t'^2}$.

$$\frac{\partial}{\partial z}\overline{w'\theta_l'} = \underbrace{-\overline{\rho}^{-1}\frac{\partial}{\partial z}(\overline{\rho}\overline{w'w'\theta_l'})}_{Turbulent Advection} \quad \underbrace{-\overline{w'^2}\frac{\partial\overline{\theta_l}}{\partial z}}_{Gradient Production}$$
$$\underbrace{+\frac{g}{\theta_{vo}}\overline{\theta_l'\theta_v'}}_{Buoyancy Production} \quad \underbrace{-\overline{\theta_l'\frac{\partial}{\partial z}\frac{p'}{\rho}}}_{Pressure} \underbrace{+\frac{\partial\overline{w'\theta_l'}}{\partial t}|_{prec}}_{Precipitation}, \quad (3.3)$$

and the equation governing the turbulent flux of r_t is written as (e.g. Khairoutdinov and Randall (2002))

$$\frac{\partial}{\partial z}\overline{w'r_t'} = \underbrace{-\overline{\rho}^{-1}\frac{\partial}{\partial z}(\overline{\rho}\overline{w'w'r_t'})}_{Turbulent Advection} \quad \underbrace{-\overline{w'^2}\frac{\partial\overline{r_t}}{\partial z}}_{Gradient Production}$$
$$\underbrace{+\frac{g}{\theta_{vo}}\overline{r_t'\theta_v'}}_{Buoyancy Production} \quad \underbrace{-\overline{r_t'\frac{\partial}{\partial z}\frac{p'}{\rho}}}_{Pressure} \underbrace{+\overline{w'\left(\frac{\partial r_t}{\partial t}\right)_{prec}}}_{Precipitation}, \quad (3.4)$$

where θ_v and θ_{vo} are virtual potential temperature and base-state virtual potential temperature, respectively.

Figure 3.8 shows the budgets of $\overline{w'\theta_l'}$ during the warm and deep phase of the simulation. The two largest terms (in magnitude) are the gradient production and buoyancy + pressure term. These two largely offset one another. Precipitation acts to increase $\overline{w'\theta_l'}$ and is maximized where the turbulent advection is negative, especially in the warm phase.

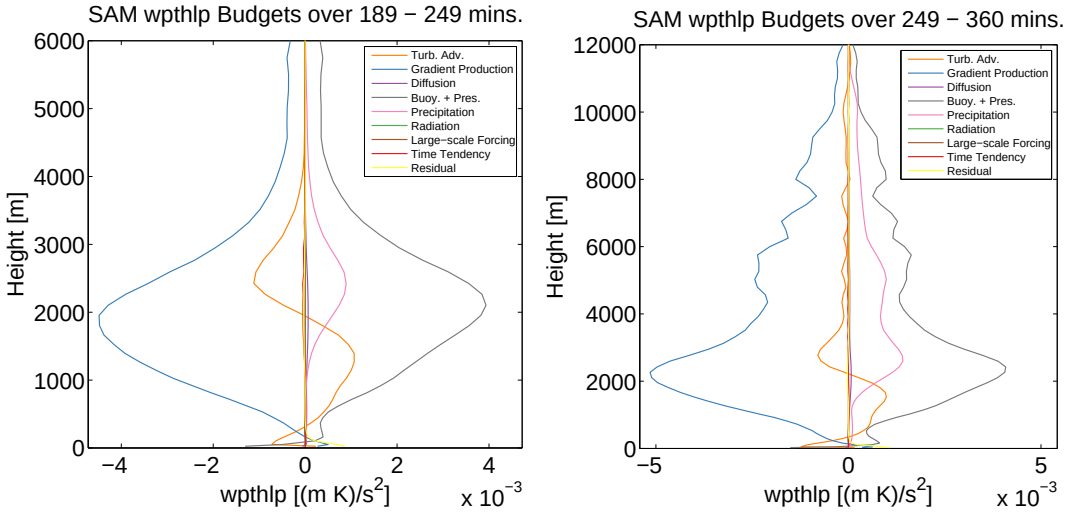

Figure 3.8: As in Figure 3.6 but for $\overline{w'\theta_l'}$.

Figure 3.9 shows the budgets of $\overline{w'r_t'}$ during the warm and deep phase of the simulation. The gradient production and buoyancy + pressure term largely offset one another. Precipitation acts as a sink of $\overline{w'r_t'}$ and is maximized where the turbulent advection is positive, especially in the warm phase.

3.2.4 Summary of the Effects of Precipitation on Higher Order Moments

For both $\overline{\theta_l'^2}$ and $\overline{r_t'^2}$ precipitation terms act as an important sink. One can imagine that the autoconversion of cloud drops to rain drops and accretion of cloud drops onto rain drops in cloudy regions ($\theta_l' < 0$) would act to remove cloud water and thus increase θ_l' closer to $\overline{\theta_l}$ and thereby reduce $\overline{\theta_l'^2}$. The same mechanism would act on $\overline{r_t'^2}$. Owing to autoconversion of cloud drops to rain drops and accretion

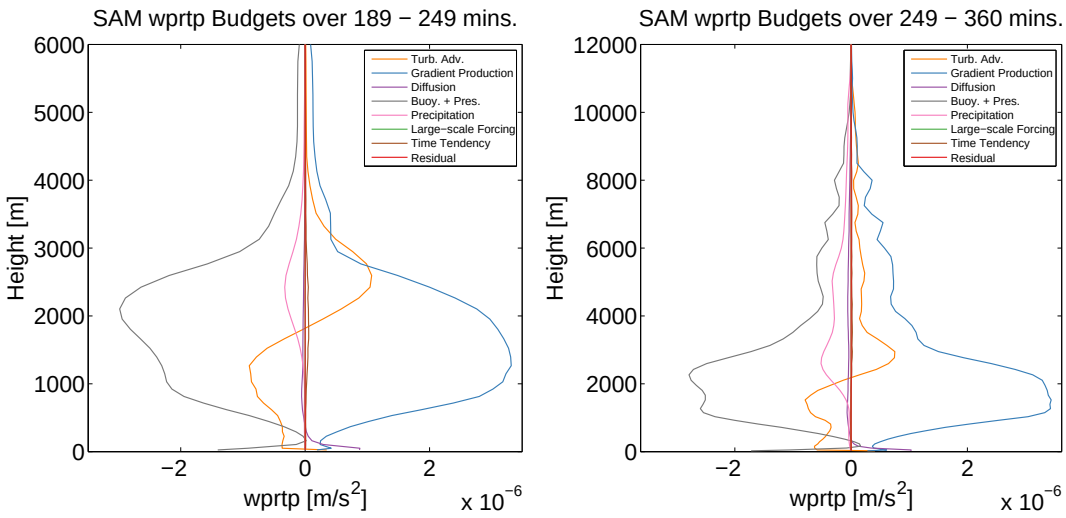

Figure 3.9: As in Figure 3.6 but for $\overline{w'r_t'}$.

of cloud drops onto rain drops, $(\frac{\partial r_t}{\partial t})$ would be negative. These processes occur in cloud, where $r_t' > 0$. Hence, precipitation acts to reduce $\overline{r'^2}$. In the budgets of $\overline{w'\theta_l'}$ and $\overline{w'r_t'}$ the buoyancy + pressure term and gradient production largely offset one another. Above cloud base, precipitation acted to oppose the turbulent advection of $\overline{w'\theta_l'}$ and $\overline{w'r_t'}$, especially in the warm phase.

The previous budget analysis shows that precipitation played an important role in the higher order moments of θ_l and r_t during a case of the transition from shallow to DMC. This is similar to the findings of Khairoutdinov and Randall (2002). They simulated 28 days with SAM using large scale forcing derived from the summer 1997 intensive observation period over the Atmospheric Radiation Measurement (ARM) Southern Great Plains (SGP) site (Zhang et al., 2001). This case is different in that the large scale forcing is weak and supplied virtually only through surface fluxes.

3.3 Semiprognostic Test: Microphysics Budgets

As seen above, rain is an important budget term in the higher order moments of θ_l and r_t. This is true even in the warm phase which is characterized by shallow clouds and light precipitation. Therefore, CLUBB's handling of the microphysical

processes of rain during the warm phase was of particular interest. Errors in CLUBB were elucidated via a semiprognostic test. As mentioned in Section 2.1, 'perfect' moments from SAM's LBA simulation were fed into CLUBB at the beginning of each CLUBB timestep. Included in the set of inputs was the mean and variance of all hydrometeors. CLUBB would then close the joint-PDF, generate 512 subcolumns, and ultimately feed each subcolumn into the same (Morrison et al., 2009) microphysics parameterization used by SAM . Microphysical budgets, including each warm rain process, were then calculated from both the SAM and CLUBB simulations leading to a straightforward comparison of the two.

Figure 3.10 shows the microphysical budget comparison of $\overline{r_r}$ and $\overline{N_r}$ for CLUBB's default configuration during the warm phase of LBA. Accretion (Accr) of cloud drops onto rains drops is overpredicted in CLUBB. Below 1500 m, the evaporation (Evap) of r_r is too low in magnitude, and too high above 1500m. The ratio, Accr:Evap, is too large below 2000 m and too small above. In the $\overline{N_r}$ budgets, the largest error is clearly the self-collection of rain drops (Self. Coll.). The large magnitude of the error illustrates a strength of the semiprognostic test. If CLUBB were run fully interactively, all the rain would quickly be depleted by excessive self-collection and this error would likely not show up.

3.3.1 Self-Collection of Raindrops

The most glaring error above was the excessive Self Coll. in CLUBB's $\overline{N_r}$ budget. Within the Morrison et al. (2009) microphysics parameterization, Self Coll. is parameterized similarly to Beheng (1994),

$$\text{Self Coll.} = -5.78 * C * \rho * N_r * r_r, \tag{3.5}$$

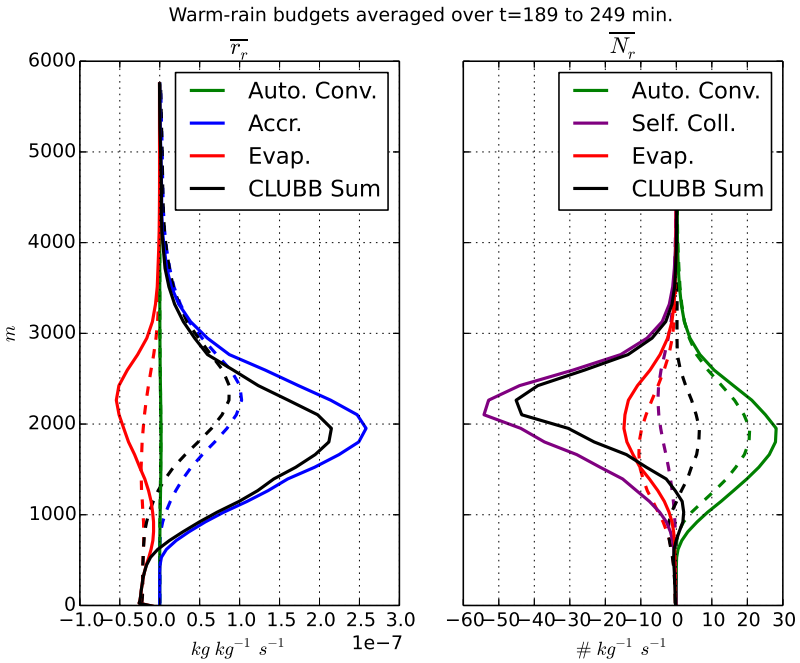

Figure 3.10: Time averaged profiles of the Morrison et al. (2009) microphysics budgets for $\overline{r_r}$ (left) and $\overline{N_r}$ (right) during the warm phase. Only the warm-rain processes are plotted. Dashed lines are budgets derived from SAM, solid lines are budgets derived from CLUBB. Autoconverion of cloud drops to rain drops ≡ Auto. Conv., accretion of cloud drops onto rain drops ≡ Accr., evaporation of rain drops ≡ Evap., self-collection of rain drops ≡ Self. Coll.. The black lines indicate the summation of the other plotted tendencies.

where C,

$$\begin{cases} C = 1 & \text{if } \frac{1}{\lambda_r} < 300 \times 10^{-6} \\ C = 2 - \exp[2300 \times (\frac{1}{\lambda_r} - 300 \times 10^{-6})] & \text{if } \frac{1}{\lambda_r} \geq 300 \times 10^{-6}, \end{cases} \tag{3.6}$$

where $\frac{1}{\lambda_r}$ is a scaled mean drop size. The inclusion of C accounts for the decreased Self Coll. efficiency with increasing mean drop size. From Equation 3.5, Self. Coll. is a largely a simple product of r_r and N_r. Figure 3.12 shows the joint-PDF of r_r and N_r at 2000 m and 225 min. into the simulation from both SAM and CLUBB. The SAM points are simply every gridpoint value from SAM's horizontal slice. Therefore, there are 16,384 points from SAM's domain and 512 samples from CLUBB's joint-PDF. Because it can be difficult to compare densities using these scatter-plots, only

512 points were colored from SAM's domain. They were colored by a relevant microphysical process (see figure captions). The CLUBB points are colored by which component of the PDF they were drawn from. In the joint-PDF of r_r and N_r, SAM shows little correlation while CLUBB shows a high correlation. Recall that CLUBB's corr(r_r,N_r) = .70 (Table 2.3). In light of SAM's joint-PDF, this appears too high.

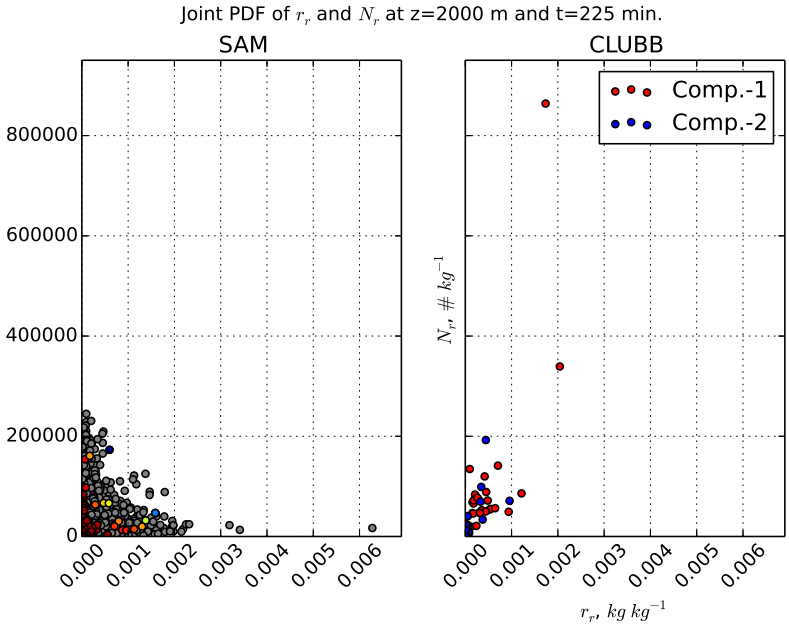

Figure 3.11: Joint-PDFs of r_r and N_r from SAM (left) and CLUBB (right) from the default configuration. Every grid point from SAM's domain is plotted, but only 512 are colored to make visual comparison easier. Cooler colors indicate larger magnitude of Self. Coll.. The CLUBB points are colored based off of which component of the PDF they are in.

3.3.2 Accretion of Cloud Drops onto Rain Drops and Evaporation of Rain Drops

Within the Morrison et al. (2009) microphysics parameterization, the accretion (Accr.) of cloud drops onto rain drops is parameterized as in Khairoutdinov and

Kogan (2000),

$$\text{Accr.} = 67 \times (r_c r_r)^{1.15}. \tag{3.7}$$

Similar to Self Coll., Accr. is a simple product between two variates, this time r_c and r_r. Recalling the convenient fact that $\chi = r_c$ when $\chi > 0.$, the joint-PDF of χ and r_r was examined. This allowed for an analysis of rain falling through cloud (accretion) and rain falling through sub saturated air (evaporation) on the same scatter-plot.

Figure 3.12 shows the joint-PDF of χ and r_r at 2000 m and 225 min. into the simulation. SAM's joint-PDF appears to have little overall correlation. CLUBB, on the other hand, has a moderate correlation. Recall that CLUBB's corr(χ,r_r) = .5 (Table 2.3).

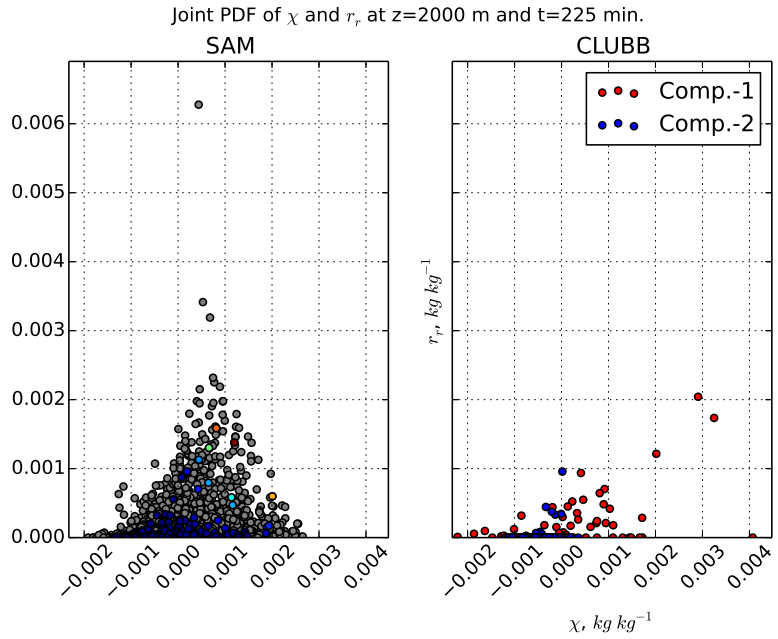

Figure 3.12: As in Figure 3.11, but for χ and r_r. Warmer colors indicate higher magnitudes of Accr.

3.3.3 New Set of Correlations

In light of the above findings, a new semiprognostic test was performed. Correlations were exactly as in Table 2.3 except: corr(χ,r_r) was decreased from .5 to .189, corr(χ,N_r) was increased from .5 to .574, and corr(r_r,N_r) was decreased from .7 to .024. Collectively, this simulation will be referred to as 'NewCorr'. The budgets from the NewCorr simulation are shown in Figure 3.13. Compared with the budgets in Figure 3.10, one can see the dramatic improvement in Self Coll. and Accr. The evaporation of $\overline{N_r}$ increased in magnitude, but was little changed in $\overline{r_r}$. Due to the reduced Self. Coll., the mean rain drop size may have remained smaller compared to the Default simulation. For an approximately equal evaporation of $\overline{r_r}$, this would cause many more rain drops to evaporate and thus increase the evaporation of $\overline{N_r}$.

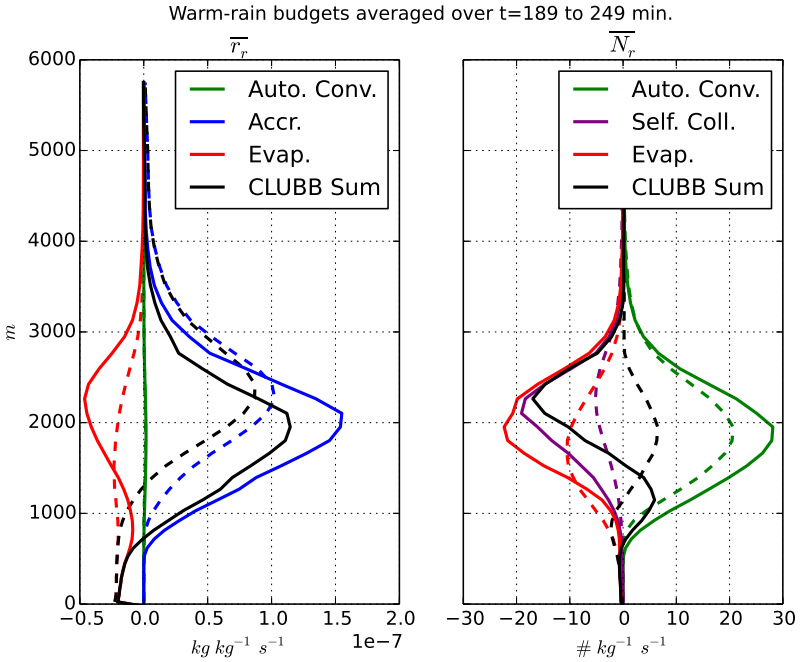

Figure 3.13: As in Figure 3.10, but for the NewCorr simulation.

By improving the correlations, improvements in the joint-PDF shape were also observed (Figures 3.14 and 3.14. However, the ratio Accr.:Evap. is still too large below 2000 m and too low above 2000 m. An improvement of this would require an improvement in the marginals. For example, in Figures 3.12 and 3.15 the first

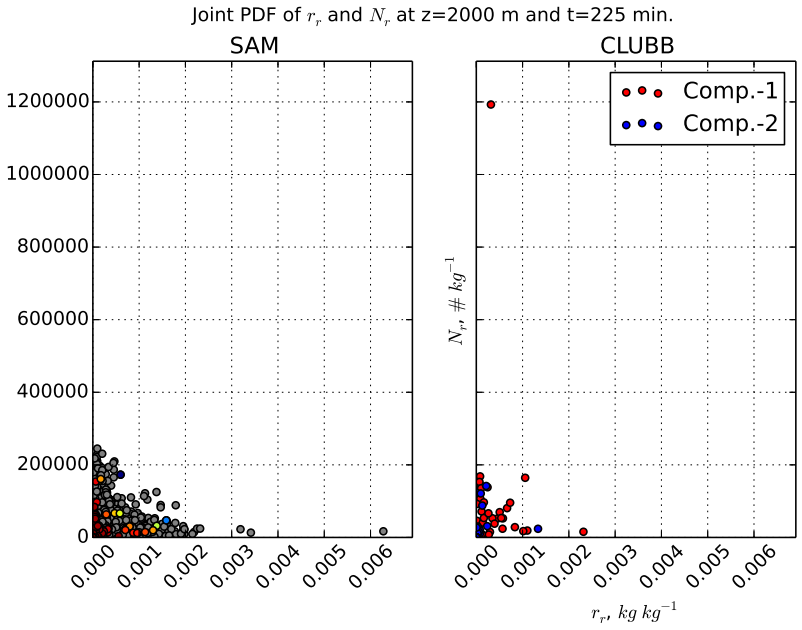

Figure 3.14: As in Figure 3.11, but for the NewCorr simulation.

component of CLUBB's marginal of χ appears too disperse. This causes rain to be found in excessively dry regions, leading to increased evaporation, and causes rain to be found in areas of high r_c, which would lead to excessive accretion. For a better illustration, Figure 3.16 shows the marginal of χ at 2000 m and 225 min. into the simulation. One can see readily that the first component is too wide with more probability mass in the extreme tails compared to SAM. What appeared to be most needed is to have the means of each χ Gaussian more different from one another. That is, the mean of the first χ Gaussian increased and its variance reduced and the mean of the second χ Gaussian decreased and its variance increased. In order to do so, however, a different strategy for closing the PDF was used as discussed below.

3.3.4 w Closure

CLUBB natively uses what is known as the the Analytic Double Gaussian 1 (ADG1) PDF (Larson et al., 2002, 2001a). As the name implies, the parameters of that PDF can be found analytically which is an attractive property. In that closure, both

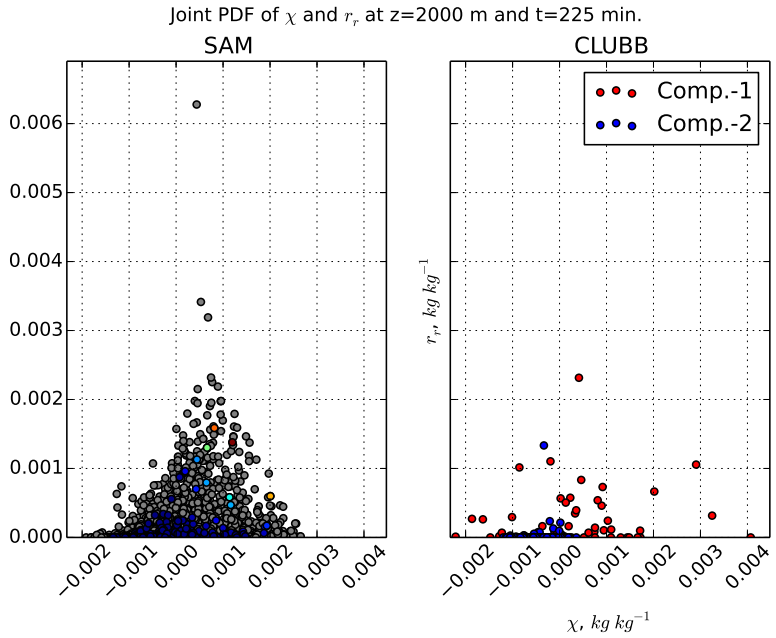

Figure 3.15: As in Figure 3.12, but for the NewCorr simulation.

widths of each w Gaussian is the same (e.g. left panel of Figure 3.17). The location and width of each w Gaussian is important since that is used to find the width and location of each θ_l and r_t Gaussians. The equations governing the mixture fraction, a, means of the i^{th} w_i component and subsequent means of the i^{th} θ_{li} component using the ADG1 closure can be found in Larson and Golaz (2005)'s Equations 20 through 25. They are,

$$a = \frac{1}{2}\left[1 - \widehat{Sk_w}\left(\frac{1}{4 + \widehat{Sk_w^2}}\right)^{1/2}\right], \tag{3.8}$$

$$\widehat{w}_1 = \frac{w_1 - \overline{w}}{\sqrt{\overline{w'^2}}}\frac{1}{(1 - \widetilde{\sigma}_w^2)^{1/2}} = \left(\frac{1-a}{a}\right)^{1/2}, \tag{3.9}$$

$$\widehat{w}_2 = \frac{w_2 - \overline{w}}{\sqrt{\overline{w'^2}}}\frac{1}{(1 - \widetilde{\sigma}_w^2)^{1/2}} = -\left(\frac{a}{1-a}\right)^{1/2}, \tag{3.10}$$

$$\widetilde{\theta}_{l1} = \frac{\theta_{l1} - \overline{\theta_l}}{\sqrt{\overline{\theta_l'^2}}} = -\frac{\widehat{c}_{w\theta_l}}{\widehat{w}_2}, \tag{3.11}$$

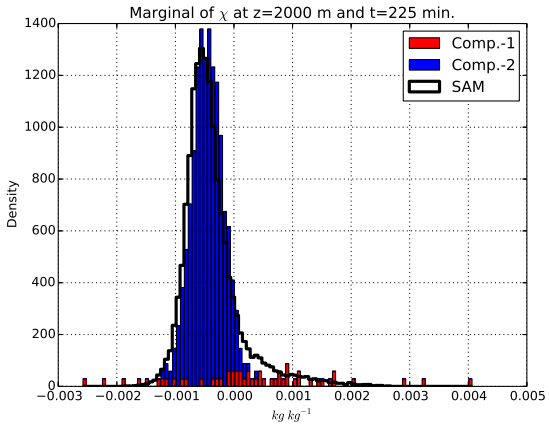

Figure 3.16: Histograms of χ from SAM (black outline) and CLUBB's sample points 225 min into the simulation at an altitude of 2000 m. The CLUBB bins are colored by the component of CLUBB's marginal they originate from.

$$\widetilde{\theta}_{l2} = \frac{\theta_{l2} - \overline{\theta_l}}{\sqrt{\overline{\theta_l'^2}}} = -\frac{\widehat{c}_{w\theta_l}}{\widehat{w}_1}, \tag{3.12}$$

where $\widetilde{\sigma}_w^2$ is the normalized variance of w, $\widehat{w}_i$ is the normalized mean of the i^{th} w Gaussian, $\widetilde{\theta_{li}}$ is the normalized mean of the i^{th} θ_l Gaussian, and $\widehat{Sk_w}$ is the normalized skewness of w. Equations for r_{ti} are analogous to those of θ_{li}.

One can see from Equations 3.11 and 3.12 that for skewed cases, such as LBA, a would decrease. During the warm phase, a minimizes at approximately .15. One can see that $\widehat{w}_1$ would take a relatively large value compared to $\widehat{w}_2$ for highly skewed cases.

The assumption that the width of each w Gaussian is the same may be too restrictive for highly skewed cases. In order for CLUBB's marginal of w to have accurate estimates of skewness may require $\widehat{w}_1$ to take on relatively extreme values. This, in turn, would cause $\widetilde{\theta}_{l1}$ and $\widetilde{\theta}_{l2}$ to be closer together. In order for $\widetilde{\theta}_{l1}$ and $\widetilde{\theta}_{l2}$ to become further apart, then $\widehat{w}_2$ and $\widehat{w}_1$ must become more similar. For example, for a fixed $\widehat{c}_{w\theta_l}$ (ultimately prescribed by SAM here, and thus known), $\widetilde{\theta}_{l1}\widehat{w}_2 = \widetilde{\theta}_{l2}\widehat{w}_1$.

Another closure, the Analytic Double Gaussian 2 (ADG2, Larson (2007); Bogenschutz et al. (2010) is the same as ADG1 except the widths of each w Gaussian

may be different. The widths of each w plume are found as in Luhar et al. (1996). The mixture fraction in ADG2 is diagnosed as,

$$a = \frac{1}{2}\left[1 - \widehat{Sk_w}\left(\frac{1}{4/M + \widehat{Sk_w^2}}\right)^{1/2}\right], \tag{3.13}$$

where,

$$M = \frac{(1+m^2)^3}{(3+m^2)^2 m^2}, \tag{3.14}$$

and

$$m = c|\widehat{Sk_w}|^{1/3}. \tag{3.15}$$

Luhar et al. (1996) set c to $\frac{2}{3}$. Here, $c = \frac{1}{2}$ was used. The widths of each w Gaussian are,

$$\widetilde{\sigma}_{w1} = \frac{\sigma_{w1}}{\sigma_w} = \left[\frac{(1-a)}{a(1+m^2)}\right]^{1/2} \tag{3.16}$$

and

$$\widetilde{\sigma}_{w2} = \frac{\sigma_{w2}}{\sigma_w} = \left[\frac{a}{(1-a)(1+m^2)}\right]^{1/2}. \tag{3.17}$$

Finally, the locations of each w Gaussian is,

$$\widetilde{w}_1 = m\widetilde{\sigma}_{w1} \tag{3.18}$$

and

$$\widetilde{w}_2 = -m\widetilde{\sigma}_{w2}. \tag{3.19}$$

Figure 3.17 shows the improvement in the marginal of w when using ADG2 versus ADG1. The marginal of θ_l is also improved, as seen in Figure 3.18. A similar improvement is seen in the marginal of r_t (not shown). The microphysical budgets using ADG2 (Figure 3.19) show a modest improvement compared to the NewCorr configuration. Evap. of $\overline{r_r}$ and $\overline{N_r}$ was reduced and Self Coll. was further reduced. What may be most promising is the overall positive tendency of $\overline{N_r}$. The profile of

Accr. looks similar to that of SAM except it is too low in altitude. Evap. or $\overline{r_r}$ is much more different between SAM and CLUBB. CLUBB's Evap. is stronger above 2000 m and much weaker below 2000 m. The ratio of Accr. to Evap. is too large below 2000 m, very similar to SAM at 2000 m., and too small above 2000 m.

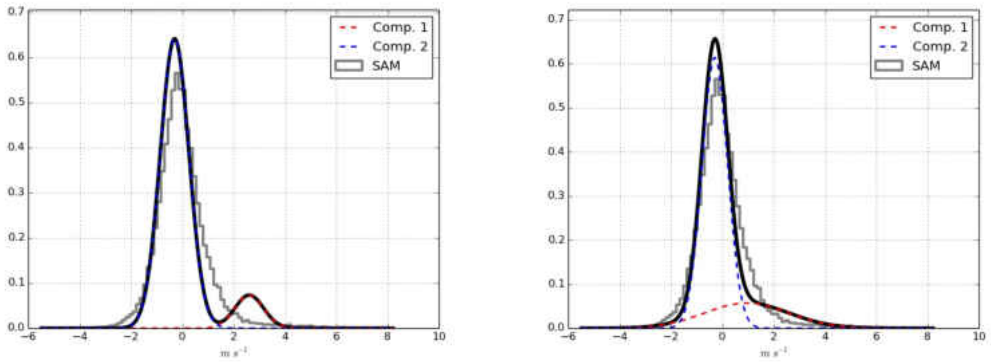

Figure 3.17: Marginals of w at 2000 m and 225 min into the simulation using ADG1 (left) and ADG2 (right). The grey outline is the histogram from SAM. The black solid line is the sum of the first (red) and second (blue) components of CLUBB's marginal.

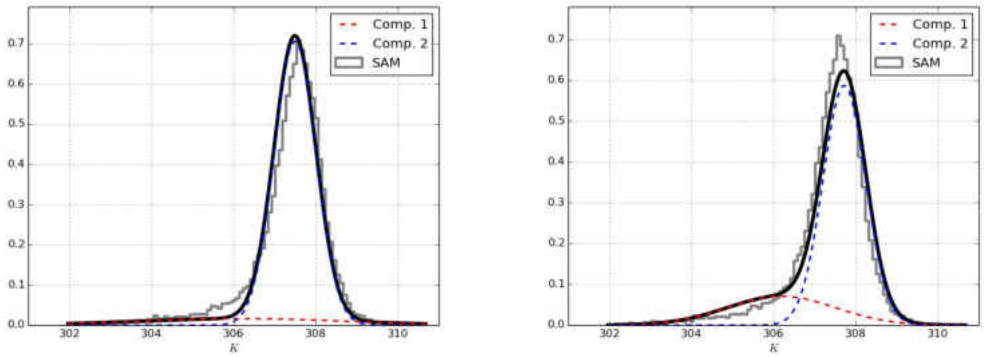

Figure 3.18: As in Figure 3.17, but for θ_l.

While ADG2 appears to improve the marginals of w, θ_l, and r_t, Accr.:Evap. is still misdiagnosed by CLUBB. Figure 3.20 shows joint-PDF's of χ and r_r and marginals of χ at 1500 m, 2000 m, and 2500 m in altitude and 225 minutes into the simulation. Shown in the plots of χ is the percent error of CLUBB's skewness of χ. Below 2000 m, the joint-PDF of χ and r_r shows almost all of CLUBB's rain

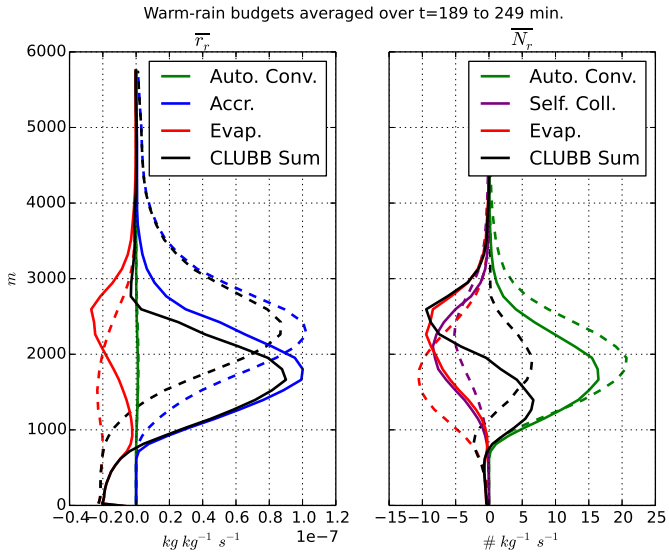

Figure 3.19: Morrison microphysical budgets, but using ADG2 and NewCorr configuration.

is found in the first component where it is more likely to fall through cloud and increase Accr.. Above 2000 m the ratio of Accr. to Evap. could also be dependent upon the skewness of θ_l and r_t and therefore χ. CLUBB underpredicts the skewness of χ at every level and the error grows with height. By 2500 m, CLUBB's skewness of χ is almost half that of SAM. Above 2000 m, this severe underprediction would result in too little Accr. and too much Evap, as seen in the joint-PDF of χ and r_r at 2500 m.

Precipitation Fraction and Skewness of θ_l and r_t

The underprediction of skewness of χ was tested. CLUBB only prognoses one third order moment, $\overline{w'^3}$. In order to close the PDF, CLUBB uses the diagnostic ansatz that the skewness of θ_l and r_t is proportional to the skewness of vertical velocity by,

$$Sk_{\theta_l} = \widehat{Sk}_w \widehat{c}_{w\theta_l} [\beta + (1-\beta)] \widehat{c}^2_{w\theta_l}, \tag{3.20}$$

where $\widehat{c}_{w\theta_l}$ is the normalized correlation of w and θ_l and β is a tunable parameter Larson et al. (2005). A similar equation holds for the skewness of r_t. In order to

ensure realizability, $0 < \beta < 3$. This ansatz was tested using regularly available output from SAM. Figure 3.21, shows SAM's skewness of θ_l and r_t and the ansatz of Equation 3.20 using SAM's moments. For each CLUBB simulation, $\beta = 2.4$. During the warm phase, Equation 3.20 appropriately diagnoses the skewness of θ_l. However, it struggles to accurately diagnose the skewness of r_t. Below 2200 m, the skewness of r_t is largely overpredicted and above 2200 m, the skewness of r_t is laregly underpredicted.

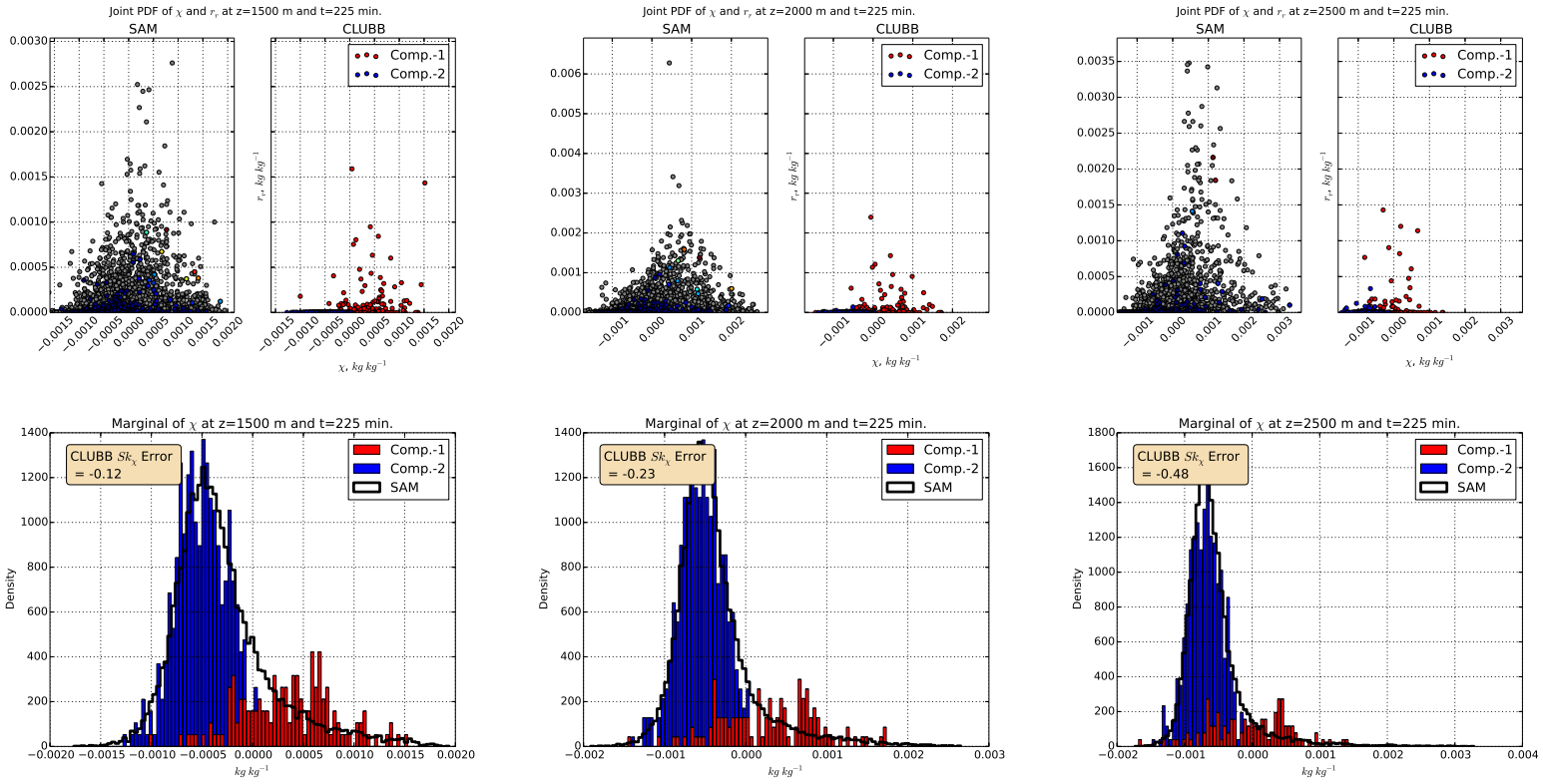

Figure 3.20: Comparisons of (top) joint-PDFs of χ and r_r and (bottom) marginals of χ for (from left to right) 1500 m, 2000 m, and 2500 m in altitude and 225 min into the simulation.

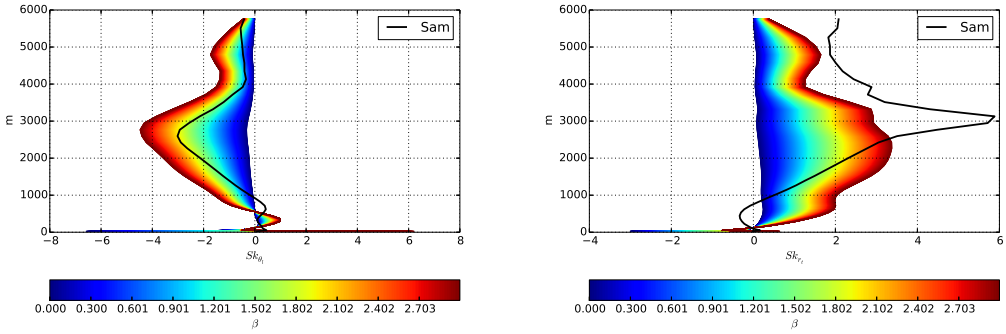

Figure 3.21: Comparison of CLUBB's ansatz for skewness of θ_l (left) and r_t (right) for the warm phase of LBA. The black line is skewness derived from SAM's simulation. Equation 3.20 is plotting across the β parameter space.

Chapter 4

Discussion and Conclusion

In the transition from shallow to DMC, precipitation plays a non-negligible role in the higher order moments involving w, r_t, and θ_l. This is true even when clouds are generally shallow and weakly precipitating. Therefore, accurately parameterizing warm rain processes appears to be necessary when parameterizing this complex transition.

Owing to CLUBB's statistical nature, detailed comparisons between CLUBB and a CRM can be done to elucidate key model errors. That advantage was used here via a semiprognostic test. From the semiprognostic test, it was show that the correlations involving hydrometeors are important factors in the microphysical budgets. CLUBB's correlation of (χ, r_r), (χ, N_r) and (r_r, N_r) should be refactored in order to produce reasonable microphysical tendencies using the Morrison et al. (2009) microphysics parameterization.

It was also shown that using the ADG2 formulation improved the marginals of w, θ_l, and r_t. However, CLUBB's profile of Accr. and Evap. was still in error. This could be due to a combination of precipitation fraction and skewness of θ_l, r_t and therefore χ. Lower in cloud, most of the precipitation was found in the first component of CLUBB's joint-PDF and thus had a greater likelihood of falling through cloud. Decreasing the precipitation fraction in the first component and increasing it in the second component of the joint-PDF may improve the ratio of Accr.:Evap. lower in cloud. Higher in cloud, the ratio may be more sensitive to the skewness of χ. CLUBB's error (underprediction) in the skewness of χ increased with height. At 2500 m, where's SAM's profile of Accr. reached a maximum, CLUBB's

skewness of χ was only about half that of SAM's. This caused more rain to fall out of cloud compared to SAM and thus, exhibit too much Evap. and too little Accr.

In a highly skewed case, such as LBA, most of the cloud and microphysical processes occur in the small tails of the joint-PDF. Thus, properly parameterizing the tails of the joint-PDF would be important. In order to do so, CLUBB must accurately prognose the skewness of w and then diagnose the skewness of θ_l, r_t. It appears that the diagnostic ansatz of Equation 3.20 breaks down in very skewed cases. Misdiagnoses of the skewness of θ_l and r_t could be a 'key' error that needs addressing as it may be a key influence on Accr.:Evap.. This may include adding prognostic equations for $\overline{\theta_l'^3}$ and $\overline{r_t'^3}$ in the future. In addition, simulations of other cloud types, and similar prognostic tests, would be needed to test the robustness of these results.

Bibliography

Arakawa, A., 2004: The cumulus parameterization problem: Past, present, and future. *J. Climate*, **17 (13)**, 2493–2525.

Beheng, K. D., 1994: A parameterization of warm cloud microphysical conversion processes. *Atmospheric Research*, **33 (1)**, 193–206.

Betts, A. and C. Jakob, 2002: Evaluation of the dirunal cycle of precipitation, surface thermodynamics, and surface fluxes in the ecmwf model using lba data. *J. Geophys. Res.*, **107**, 12–1 – 12–3.

Bogenschutz, P. A., A. Gettelman, H. Morrison, V. E. Larson, C. Craig, and D. P. Schanen, 2013: Higher-order turbulence closure and its impact on climate simulations in the Community Atmosphere Model. *J. Climate*, **26**, 9655–9676, doi: doi:10.1175/JCLID-13-00075.1.

Bogenschutz, P. A., S. K. Krueger, and M. Khairoutdinov, 2010: Assumed probability density functions for shallow and deep convection. *J. Adv. Model. Earth Syst.*, **2**, doi:10.3894/JAMES.2010.2.10.

Boucher, O., et al., 2013: Clouds and aerosols. *Climate Change 2013: The Physical Science Basis. Contribution of Working Group I to the Fifth Assessment Report of the Intergovernmental Panel on Climate Change*, T. F. Stocker, D. Qin, G.-K. Plattner, M. Tignor, S. K. Allen, J. Boschung, A. Nauels, Y. Xia, V. Bex, and P. Midgley, Eds., Cambridge University Press, Cambridge, United Kingdom and New York, NY, USA.

Bryan, G. H., J. C. Wyngaard, and J. M. Fritsch, 2003: Resolution requirements for the simulation of deep moist convection. *Mon. Wea. Rev.*, **131 (10)**, 2394–2416.

Golaz, J.-C., V. E. Larson, and W. R. Cotton, 2002: A PDF-based model for boundary layer clouds. Part I: Method and model description. *J. Atmos. Sci.*, **59**, 3540–3551.

Grabowski, W. W., et al., 2006: Daytime convective development over land: A model intercomparison based on LBA observations. *Quart. J. Roy. Meteor. Soc.*, **132**, 317–344.

Griffin, B. M. and V. E. Larson, 2013: Analytic upscaling of local microphysics parameterizations, Part II: Simulations. *Quart. J. Royal Met. Soc.*, **139**, 58–69.

Jakob, C., 2010: Accelerating progress in global atmospheric model development through improved parameterizations: challenges, opportunities, and strategies. *Bull. Amer. Meteor. Soc.*, **91**, 869875.

Jakob, C., 2014: Going back to basics. *Nature Climate Change*, **4**, 1042–1045.

Khairoutdinov, M. and Y. Kogan, 2000: A new cloud physics parameterization in a large-eddy simulation model of marine stratocumulus. *Mon. Wea. Rev.*, **128**, 229–243.

Khairoutdinov, M., S. K. Krueger, C.-H. Moeng, P. A. Bogenschutz, and D. A. Randall, 2009: Large-eddy simulation of maritime deep tropical convection. *Journal of Advances in Modeling Earth Systems*, **1 (15)**, 13 pp.

Khairoutdinov, M. and D. A. Randall, 2002: Similarity of deep continental cumulus convection as revealed by a three-dimensional cloud-resolving model. *J. Atmos. Sci.*, **59**, 2550–2566.

Khairoutdinov, M. and D. A. Randall, 2003: Cloud resolving modeling of the ARM Summer 1997 IOP: Model formulation, results, uncertainties, and sensitivities. *J. Atmos. Sci.*, **60**, 607–624.

Khairoutdinov, M. and D. A. Randall, 2006: High-resolution simulation of shallow-to-deep convection transition over land. *J. Atmos. Sci.*, **63 (12)**, 3421–3436.

Larson, V. E., 2007: From cloud overlap to PDF overlap. *Quart. J. Royal Met. Soc.*, **133**, 1877–1891, doi:10.1002/qj.165.

Larson, V. E. and J.-C. Golaz, 2005: Using probability density functions to derive consistent closure relationships among higher-order moments. *Mon. Wea. Rev.*, **133**, 1023–1042.

Larson, V. E., J.-C. Golaz, and W. R. Cotton, 2002: Small-scale and mesoscale variability in cloudy boundary layers: Joint probability density functions. *J. Atmos. Sci.*, **59**, 3519–3539.

Larson, V. E., J.-C. Golaz, H. Jiang, and W. R. Cotton, 2005: Supplying local microphysics parameterizations with information about subgrid variability: Latin hypercube sampling. *J. Atmos. Sci.*, **62**, 4010–4026.

Larson, V. E. and B. M. Griffin, 2013: Analytic upscaling of local microphysics parameterizations, Part I: Derivation. *Quart. J. Royal Met. Soc.*, **139**, 46–57.

Larson, V. E. and D. P. Schanen, 2013: The Subgrid Importance Latin Hypercube Sampler (SILHS): a multivariate subcolumn generator. *Geosci. Model Dev.*, **6**, 1813–1829, doi:10.5194/gmdd-6-1813-2013.

Larson, V. E., D. P. Schanen, M. Wang, M. Ovchinnikov, and S. Ghan, 2012: PDF parameterization of boundary layer clouds in models with horizontal grid spacings from 2 to 16 km. *Mon. Wea. Rev.*, **140**, 285–306.

Larson, V. E., R. Wood, P. R. Field, J.-C. Golaz, T. H. Vonder Haar, and W. R. Cotton, 2001a: Small-scale and mesoscale variability of scalars in cloudy boundary layers: One-dimensional probability density functions. *J. Atmos. Sci.*, **58**, 1978–1994.

Larson, V. E., R. Wood, P. R. Field, J.-C. Golaz, T. H. Vonder Haar, and W. R. Cotton, 2001b: Systematic biases in the microphysics and thermodynamics of numerical models that ignore subgrid-scale variability. *J. Atmos. Sci.*, **58**, 1117–1128.

Lewellen, W. S. and S. Yoh, 1993: Binormal model of ensemble partial cloudiness. *J. Atmos. Sci.*, **50 (9)**, 1228–1237.

Luhar, A. K., M. F. Hibberd, and P. J. Hurley, 1996: Comparison of closure schemes used to specify the velocity PDF in Lagrangian stochastic dispersion models for convective conditions. *Atmos. Environ.*, **30**, 1407–1418.

Morrison, H., G. Thompson, and V. Tatarskii, 2009: Impact of cloud microphysics on the development of trailing stratiform precipitation in a simulated squall line: Comparison of one- and two-moment schemes. *Mon. Wea. Rev.*, **137**, 993–1009.

Randall, D., M. Khairoutdinov, A. Arakawa, and W. Grabowski, 2003: Breaking the cloud parameterization deadlock. *Bull. Amer. Meteor. Soc.*, **84 (11)**, 1547–1564.

Randall, D. A., 2013: Beyond deadlock. *J. Geophys. Res.*, **40**, 5970–5976.

Randall, D. A., D.-M. Pan, P. Ding, and D. G. Cripe, 1997: Quasi-equilibrium. *The Physics and Parameterization of Moist Atmospheric Convection*, R. K. Smith, Ed., Kluwer Academic Publishers, 359–385.

Silva Dias, M. A. F., et al., 2002: Cloud and rain processes in a biosphere-atmosphere interaction context in the Amazon region. *J. Geophys. Res.*, **107 (D20)**, 8072.

Storer, R., B. Griffin, J. Höft, J. Weber, E. Raut, V. Larson, M. Wang, and P. Rasch, 2015: Parameterizing deep convection using the assumed probability density function method. *Geoscientific Model Development*, **8 (1)**, 1–19.

Zhang, M. H., J. L. Lin, R. T. Cederwall, J. J. Yio, and S. C. Xie, 2001: Objective analysis of the ARM IOP data: Method and sensitivity. *Mon. Wea. Rev.*, **129**, 295–311.

Zhang, Y. and S. A. Klein, 2010: Mechanisms affecting the transition from shallow to deep convection over land: inferences from observations of the diurnal cycle collected at the arm southern great plains site. *J. Atmos. Sci.*, **67**, 2943–2959.